Visualizing magnetic control of nanoparticles for airway gene therapy using ultrafast *in vivo* dark-field X-ray imaging

Cystic fibrosis is the most common life-limiting genetic disorder in Australia, with respiratory disease the leading cause of mortality. Cystic fibrosis is caused by a mutation of the *CFTR* gene, so a proposed treatment strategy is gene-addition therapy, whereby fully functioning copies of the *CFTR* gene are delivered to cells using a transfer vector. Gene vectors need to be transported to the specific airway cells that require correction, and retained in place long enough to interact with those cells. This is made challenging by mucociliary clearance, a process that traps inhaled particles in mucus and clears them from the airways via ciliary motion. A novel approach to overcome these challenges is coupling the gene vector to magnetic nanoparticles, allowing the vector to be retained and controlled within the airways using external magnetic fields [1].

Controlling and visualizing magnetic nanoparticle behavior within airways is challenging. Previously, propagation-based phase-contrast X-ray imaging showed magnetic nanoparticles form strings in the airway under exposure to a magnetic field, but these are very hard to visualize. Here we have explored the use of dark-field X-ray imaging to further enhance nanoparticle contrast and gain new insights into magnetic particle control *in vivo*. X-ray dark-field imaging detects ultra-small angle scattering caused by microstructures within the sample [2]. If these structures are asymmetric and the longest axes are aligned, they can scatter anisotropically (i.e., X-rays are scattered preferentially in one direction, usually orthogonal to the orientation of the scattering object). Detecting this scatter gives the directional dark-field signal [2], allowing the orientation of microstructures to be measured.

The aim of this study was to explore how magnetic nanoparticles behave within a live airway under the influence of dynamic magnetic fields. We hypothesized that the directional X-ray dark-field signal could help visualize the presence of the nanoparticles, showing how they move in response to the magnetic field.

The experiment was undertaken at SPring-8 **BL20XU** beamline. A rat was anaesthetized and a cannula inserted into the trachea to enable delivery of magnetic nanoparticles to the airways using a syringe pump. A 3D-printed motorized magnet holder, shown

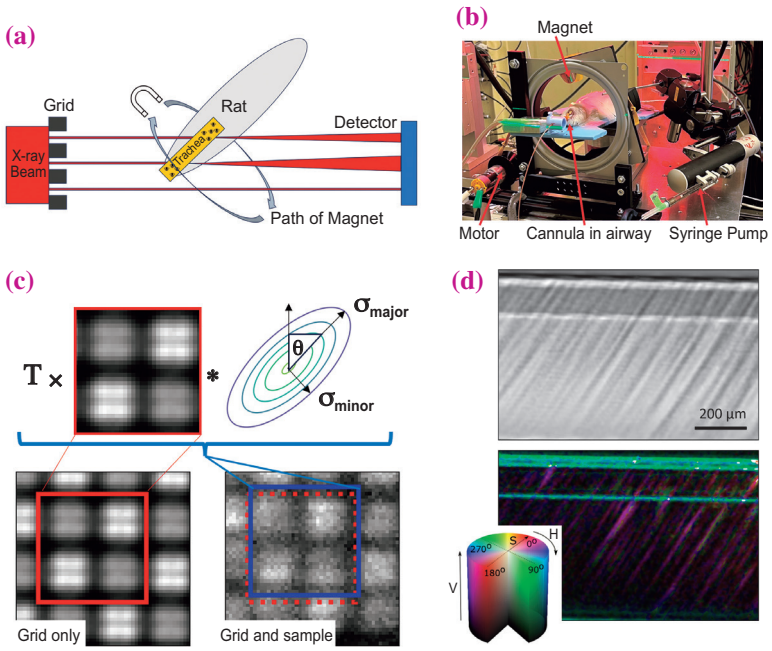

Fig. 1. **(a)** Shows a simplified top-down view of the experiment. The beam is patterned by a phase grid, creating beamlets. These beamlets are diffused as they scatter through the sample, with the dark-field extracted from the strength of the blurring seen downstream at the detector. **(b)** A photo of the motorized magnetic array and rat. **(c)** Shows how the blurring of the beamlets is modelled by the UMPA algorithm, using an intensity scaling for transmission T, and convolution with a directional dark-field kernel. **(d)** Shows that magnetic nanoparticles in a capillary tube (shown in transmission in the upper image) produce a directional dark-field signal (lower image). [3]

in Fig. 1(b) was designed to externally rotate a magnet around the rat.

To extract the X-ray dark-field signal, a checkerboard phase grid was placed into the beam upstream of the sample. Figure 1(a) shows a simplified diagram of the grid producing a pattern of beamlets, with the sample scattering each beamlet. The dark-field images were extracted using the directional dark-field extension to the unified modulation pattern analysis (UMPA) algorithm [2]. UMPA compares windows in the grid pattern with and without the sample in the beam. Attenuation is measured by looking at the reduction of intensity, and phase can be found by looking at how the beamlets are refracted. The directional dark-field signal is modelled as the blurring of the pattern by a two-dimensional Gaussian kernel (Fig. 1(c)).

Images were taken of 'strings' of magnetic nanoparticles in a capillary tube to confirm that they produced a directional dark-field signal (Fig. 1(d)). The directional dark-field image uses a HSV color scheme. The hue (H) relates to the scattering orientation θ and the saturation (S) to the eccentricity of the Gaussian kernel. The value (V) is the scattering magnitude.

Images of the particles during delivery were used to quantify the contrast enhancement of dark-field imaging compared to the attenuation signal. The transmission value decreased by 5.2 standard deviations from the mean background value, while the dark-field signal peaked at 18.6 standard deviations from the background signal, showing that dark-field increased the signal-to-noise ratio of this event 3.5-fold.

Having seen that adding an external magnetic field causes the magnetic nanoparticles to create packed string-like structures, we then rotated a magnet around the outside of the rat's neck to cause these strings to form and rotate within the trachea. Figure 2 shows images of a highly concentrated region of magnetic nanoparticles as the field changes, with a directional dark-field clearly visible. However, in regions with a lower concentration of magnetic nanoparticles, the directional dark-field signal was not as clear. Although we have shown proof-of-concept for *in vivo* directional dark-field airway imaging, we expect that further optimization of the imaging setup will enhance contrast further. This will allow us to continue our goal of developing magnetically guided airway gene therapy treatments.

All animal studies were performed in accordance with protocols approved by the University of Adelaide and SPring-8 animal ethics committees.

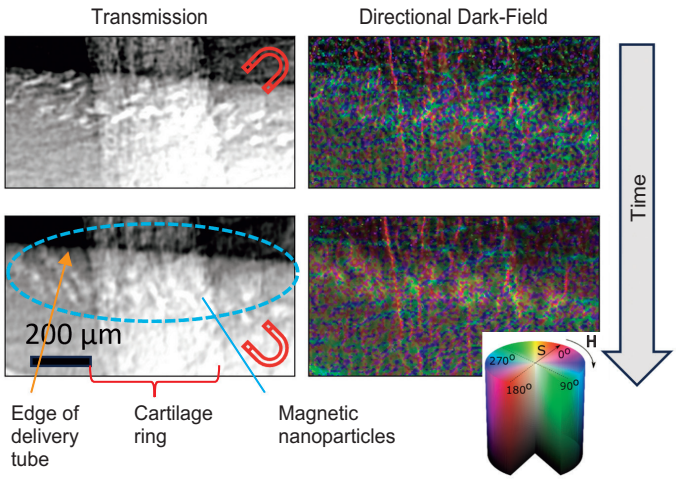

Fig. 2. X-ray transmission and directional dark-field images taken from a time series as the magnet passes around the rat (magnet symbol shows the approximate direction of magnetic field). [3]

Ronan Smith[a,*], Kaye Morgan[b] and Martin Donnelley[a]

[a] Adelaide Medical School, University of Adelaide, Australia
[b] School of Physics and Astronomy, Monash University, Australia

*Email: ronan.smith@adelaide.edu.au

References

[1] M. Donnelley *et al.*: Sci. Rep. **12** (2022) 9000.
[2] A. C. J. Smith *et al.*: PLoS One **17** (2022) e0273203.
[3] *R. Smith, K. Morgan, A. McCarron, P. Cmielewski, N. Reyne, D. Parsons and M. Donnelley: Phys. Med. Biol.* ***69*** *(2024) 105025.*